Lab on a Chip

Cite this: *Lab Chip*, 2012, **12**, 2903–2908

www.rsc.org/loc

PAPER

Force driven separation of drops by deterministic lateral displacement

Timothy Bowman, Joelle Frechette* and German Drazer*

Received 6th March 2012, Accepted 18th April 2012
DOI: 10.1039/c2lc40234c

We investigate the separation of drops in force-driven deterministic lateral displacement (*f*-DLD), a promising high-throughput continuous separation method in microfluidics. We perform scaled-up macroscopic experiments in which drops settle through a square array of cylindrical obstacles. These experiments demonstrate the separation capabilities—and provide insight for the design—of *f*-DLD for drops of multiple sizes, including drops that are larger than the gaps between cylinders and exhibit substantial deformation as they move through the array. We show that for any orientation of the driving force relative to the array of obstacles, the trajectories of the drops follow selected locking directions in the lattice. We also found that a simple collision model accurately describes the average migration angles of the drops for the entire range of sizes investigated here, and for all forcing directions. In addition, we found a difference of approximately 20° between the critical angles at which the smallest and largest drops first move across a line of obstacles (column) in the array, a promising result in terms of potential size resolution of this method. Finally, we demonstrate that a single line of cylindrical obstacles rotated with respect to the driving force is capable of performing binary separations. The critical angles obtained in such single line experiments, moreover, agree with those obtained using the full array, thus validating the assumption in which the trajectory (and average migration angle) of the drops is calculated from individual obstacle-drop collisions.

1. Introduction

The quest to separate and analyse chemical species with higher resolution, sensitivity, and throughput has been central to the development of microfluidics systems since their origin.[1,2] Separation systems are also a unit operation that is at the core not only of micro-total-analysis systems[3–5] (μ-TAS) but also for lab-on-a-chip integration efforts in general.[6] In fact, a number of different separation strategies have been developed in recent years for microdevices with a variety of applications.[7] In the design of separation schemes, continuous flow systems are favoured, both for integration purposes and because they typically offer higher throughput.[8–11] Deterministic lateral displacement (DLD) is a separation method with these capabilities that has shown great potential for the fractionation of suspended particles in different biological areas, ranging from tissue-engineering to diagnostics.[12–21] In DLD, a suspension is driven though an array of obstacles and the different components move in locked-in trajectories, migrating at different angles. Interestingly, higher velocities show sharper size resolution, which suggests that this method operates in a deterministic fashion, and is therefore compatible with higher throughput than comparable stochastic methods.[12,22] In addition, the two-dimensional nature of DLD offers the possibility of improved spatial resolution, compared to traditional one-dimensional methods. Another important advantage of DLD is that the suspension is fractionated without altering the native state of the different species.[23] Finally, DLD is a passive or fluidic-only technique, in that it simply relies on the geometry of the stationary media and the properties of the flow to separate the sample, without the need of external fields.[24]

In the original DLD work, the geometry consisted of a square array of cylindrical obstacles rotated with respect to the flow direction.[12] The authors observed two types of motion for suspended particles: a *displacement* or *bumping* mode in which relatively large particles would stay in the same lane between columns of obstacles and therefore move at an average angle $\alpha = 0^\circ$ with respect to the array; and a *zigzag* or *streamline* mode in which smaller particles followed the flow direction on average, crossing a column of obstacles every 10 rows. (Analogous results were reported using an oblique lattice with the angle of the lattice being the same as the rotation angle above.[25]) Recent work has shown that in fact there could be multiple sorting directions (mixed motion), which is advantageous for separation purposes.[26–28] We have observed analogous behaviour in macroscopic experiments, using a scaled-up version of a DLD device, when the particles are driven through the array of obstacles by a constant force[29] (*f*-DLD). The particles also exhibit directional locking, on average migrating at selected lattice directions. Directional-locking is also observed in the motion of a particle through a square lattice of repulsive centres.[30] Our macroscopic experiments not only established the deterministic nature of the

Chemical and Biomolecular Engineering Department, Johns Hopkins University, 3400 N. Charles St., Baltimore, MD 21218
E-mail: frechette@jhu.edu; drazer@jhu.edu

observed directional locking, but also showed the importance of irreversible particle–obstacle interactions as the underlying mechanism leading to migration angles that are different from the driving direction. Recently, scaled-up experiments were also used to investigate the performance of DLD devices at large particle volume fractions.[31]

One of the driving forces in the development of microfluidic separation systems is the growing interest in lab-on-a-chip devices for cell manipulation and analysis.[11,23] The progress and potential of droplet-based microfluidics,[32,33] has motivated the investigation of different techniques for the separation of drops and multiphase fluids. [34–37] However, in contrast to the case of colloidal particles, the motion of deformable components in DLD devices has not been investigated in detail.[19,38,39] A recent study reported, for the first time, good size-separation of a binary sample of 30 μm and 11 μm (water based) droplets in oil,[19] and simulation of elastic capsules yielded similar results[38]. Beyond lab-on-a-chip technologies, the separation of the different components in multiphase flows is at the heart of a number of engineering applications, ranging from enhanced oil production to emulsions.

Here, we first demonstrate the separation capabilities of *f*-DLD for several drop sizes, from relatively small ones that easily move through the device, to large drops that exhibit substantial deformation as they move through the array. We investigate the entire range of forcing angles and establish the presence of directional locking analogous to that observed for rigid particles. In fact, for the entire range of forcing directions and for all drop sizes a simple collision model developed to describe the motion of rigid particles accurately describes the locking observed in the average migration angle of drops. We also demonstrate that differences in the average velocities of different size drops can be employed, along with the lateral displacement, to enhance the separation capabilities of *f*-DLD. Finally, and for the first time, we show that a single line of cylindrical obstacles, slanted with respect to the driving force, is capable of performing binary separations, and that the results can be predicted based on the array experiments and *vice versa*. Our large data set indicates that the first critical angle, at which a given drop size becomes unlocked from moving down a single column (see Fig. 1), depends linearly on size. In addition, we observe a window of approximately 20° for the first critical angles for the drops considered here, a promising result in terms of the potential drop–size resolution of *f*-DLD.

2. Experimental results and discussion

2.1 Experimental setup and characteristic parameters

The deterministic character of DLD allows us to investigate the separation of drops by means of experiments in a scaled-up macroscopic device (Pe $\gg$ 1). Specifically, we use an array of obstacles created with cylindrical LEGO® pegs positioned in a square lattice on a LEGO® board (Fig. 1). The array is immersed in a transparent tank filled with oil and aligned vertically such that gravity is in the plane of the array. A continuous train of monodisperse water drops is created using a syringe and introduced from the top of the tank, such that they move through the array as they settle under gravity. The forcing angle is controlled by rotating the LEGO® board. We measure both the forcing angle (θ) and the migration angle (α) relative to one of the principal axis of the array, say the *y*-axis, as shown in Fig. 1. Then, $\theta = 0°$ for example, corresponds to the *y*-axis aligned with the direction of gravity. Note that due to the high symmetry of the square array all the forcing directions are covered with $\theta = 0°$–45°. Fig. 1 presents two different trajectories showing the separation of 7.5 mm and 5.3 mm drops.

To scale up the microfluidic DLD devices, possible inertia effects are reduced using a viscous oil ($\mu \approx 6 \times 10^{-2}$ Pa s, $\gamma \approx 3 \times 10^{-2}$ N m^{-1}) and the Reynolds number ranges from Re $\approx$ 0.1 to Re $\approx$ 2, the latter calculated for the largest drops ($a \approx 6$ mm) and using their largest settling velocity ($U \approx 20$ mm s^{-1} for $\theta \approx 0°$). The capillary numbers are also small in all the experiments presented here, with Ca $< 5 \times 10^{-2}$, which is consistent with microfluidics.[40,41] The ratio between the diameter of the obstacles ($2R = 7.8$ mm) and the lattice spacing ($l = 16$ mm) is $\lambda = 2R/l = 0.49$. We normalize the drop radius with the obstacle radius, $\beta = a/R$. In the experiments discussed here, β ranges from 0.47 to 1.5. Finally, it is also important to compare the size of the drop with the gap between pegs, $\Delta = l - 2R$, which, when normalized by the diameter of the obstacles, becomes, $\delta = \Delta/2R = \lambda^{-1} - 1 = 1.05$. Therefore, for $\beta > \delta = 1.05$ the drops do not fit through the gap between the pegs unless they deform.

2.2 Migration experiments

In Fig. 2 we plot the average migration angle, α, as a function of the forcing angle, θ, for drops that easily fit through the gap between obstacles ($\beta \approx 0.5\delta$) to large drops that show significant deformations as they move through the array ($\beta \approx 1.5\delta$). The dependence of the migration angle on the forcing angle resembles that observed for solid particles, with regions of constant migration angle followed by sharp transitions between them. These 'Devil's staircases' are a characteristic feature of systems exhibiting directional locking.[42] The locking directions (plateaus of constant migration angle) correspond to lattice directions of the array. For example, the smallest drops are the first to transition from the locking direction [0,1] to the [1,3] lattice direction. When locked into the [0,1] direction, the falling drop settles along a single column of the array, on average moving only in the *y*-axis. The [1,3] locking direction corresponds to a more complex motion in which the drops change column every 3 rows. The fact that, for a given forcing direction, the migration angles of different size drops are in general different indicates that a mixture of drops would spontaneously separate as they move through the device. Although the results presented in Fig. 1 mostly indicate the possibility of binary separation, in that drops of different size would be separated into two groups settling at two different migration angles, there is a small window of forcing angles, $\theta \approx 30°$, for which three migration angles are observed simultaneously, corresponding to the [0,1], [1,2], and [1,1] lattice directions.

More importantly, and also consistent with our observations in the case of solid particles, the first critical angle θ_c shows the strongest dependence on size,[29] with a range of nearly 20° for the range of drops sizes considered here. Interestingly, the first critical angle exhibits a linear dependence on the drop size over the entire range, including the large, deforming drops (see

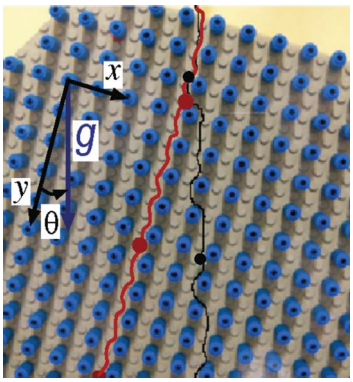

Fig. 1 Picture of the experimental setup showing the LEGO® board and the cylindrical pegs forming a square array rotated at an angle $\theta = 18^\circ$ with respect to gravity. We also overlaid the trajectory followed by two types of drops, 3.75 mm (shown in red) and 2.65 mm drops (shown in black). Clearly, the larger drops are locked in the [0,1] direction, and sediment along a single column in the array, whereas the smaller drops are able to change columns and move in a direction closer to the force, with $\alpha = 18.4^\circ$, corresponding to the [1,3] direction.

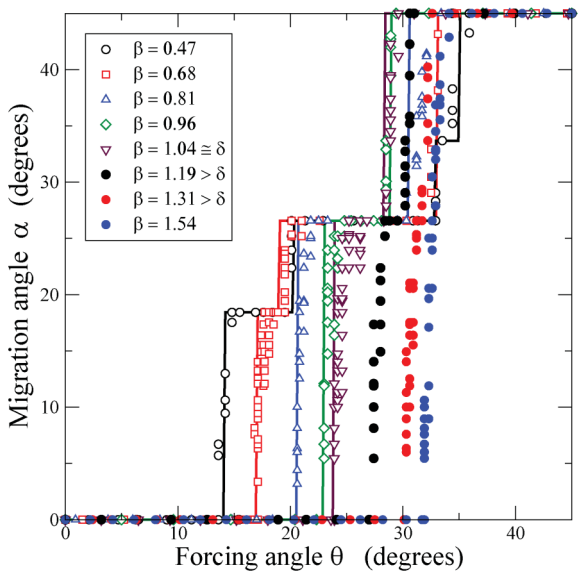

Fig. 2 Migration angle α as a function of the forcing angle θ for drops of different size. The open (solid) symbols correspond to drops of sizes $\beta < \delta$ ($\beta > \delta$). The solid lines correspond to the model, with b_c obtained from the first transition.

Fig. 3). This linear dependence would be particularly useful in the design of obstacle arrays for separation devices as it adds predictability and facilitates calibration. On the other hand, this is an empirical observation that would need to be validated for different materials and in the actual microdevices.

In Fig. 4 we present the average settling velocity of the drops as a function of the forcing direction. It is clear that, for a given forcing angle θ, drops of different sizes settle at different velocities, and a mixture of them will also separate even if they move in the same direction. For example, consider a forcing angle $\theta = 23^\circ$ and a mixture of 3.7 mm, 6.3 mm, 8.1 mm and 10.2 mm drops. The two smallest drops will move in the [1,2] direction, but the velocity of the 6.3 mm would be nearly twice

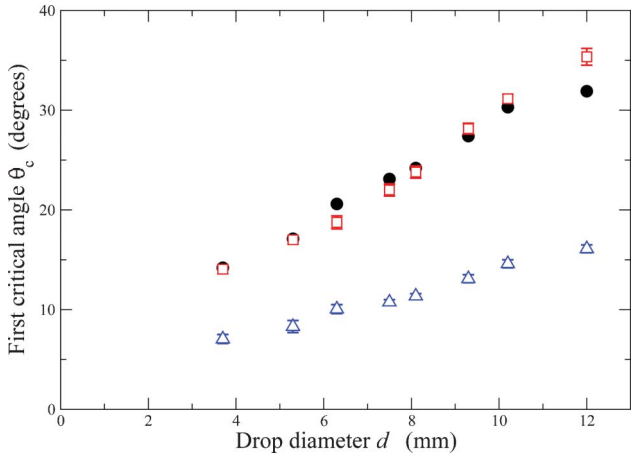

Fig. 3 First critical angle as a function of drop size. The solid symbols correspond to the first critical angle measured in the LEGO® system. The open squares (triangles) correspond to a single arrow of obstacles with separation l ($2l$).

that of the 3.7 mm drops. Similarly, the two largest drops would still be locked into the [0,1] direction, but the 10.2 mm drops will move substantially faster than the 8.1 mm ones. It is also clear from Fig. 4 that the settling velocity of the drops decreases significantly as the forcing direction approaches the transition angles, in agreement with simulation results obtained for solid particles when particle-obstacle hydrodynamic interactions are included.[43] In fact, the lubrication forces that reduce the mobility of a solid particle close to the obstacles are also present in the case of a drop moving close to a solid surface. We note that the variations in settling velocity may result, for some orientation angles, in smaller drops settling faster than larger ones. The settling speed is also affected by the aspect ratio between the drop size and the open gap between obstacles, β/δ. In fact, we see that the settling velocity at zero forcing angle is clearly not monotonic. In the inset of Fig. 4 we plot the settling velocity as a function of the forcing direction shifted by the first critical angle, $(\theta-\theta_c)$. It is clear that the dependence of the settling velocity on

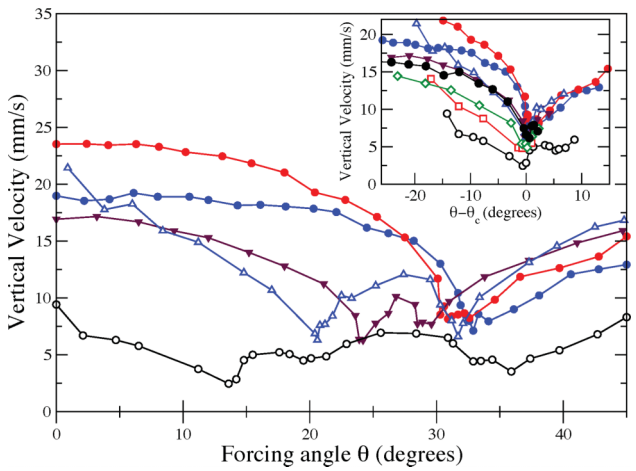

Fig. 4 Drops velocity along the forcing direction as a function of the forcing angle. The symbols are the same as in Fig. 2. The inset shows the same data but plotted around the critical angle for each drop.

this shifted forcing angle is similar for all drop sizes, with a critical slowdown as the forcing direction approaches θ_c.

2.3 Dilute limit model of deterministic lateral displacement

In our previous work, we demonstrated that the motion of suspended solid particles in periodic systems could be described from the motion of a single particle past a fixed obstacle, which we referred to as a particle–obstacle collision.[29,44] Moreover, our previous experimental results were in excellent agreement with a simple particle-obstacle collision model in which the effect of all irreversible forces is represented by a hard-core repulsion with range $(1 + \varepsilon)\ a$, where ε can be considered as an effective roughness.[29] In this model there are only two type of collisions: (i) simple, hydrodynamic collisions, in which the distance between the particle and the obstacle is never smaller than εa, and (ii) touching collisions, in which the particle reaches the minimum separation εa during the approaching part of the trajectory and the hard-core repulsion prevents the particle from getting closer to the obstacle. The hydrodynamic collisions are reversible in the absence of inertia (and deformation) and, as a result, there is no net lateral displacement. In other words, the initial offset, or incoming impact parameter b_{in}, is the same as the outgoing impact parameter b_{out}. The impact parameter is defined as the distance between the asymptotic line of motion of the particle and the parallel line that goes through the centre of the obstacle (see Fig. 5). In the case of touching collisions the hard-core repulsion prevents the approaching particles from getting closer than $(1 + \varepsilon)a$ but has no effect as they move apart and, as a result, the trajectories are not symmetrical and lead to a net lateral displacement. This lateral displacement experienced at each particle-obstacle touching collision accumulates as the particle moves through the periodic array and leads to the observed difference between the forcing and migration angles. Touching collisions result whenever the incoming impact parameter (b_{in}) is smaller than a critical value, b_c, which corresponds to the impact parameter that leads to a minimum particle-obstacle gap equal to εa, in the absence of the repulsive interaction. Examples of both hydrodynamic and touching collisions are schematically shown in Fig. 5. All the touching collisions collapse into a single outgoing trajectory with $b_{out} = b_c$. In a separate study we showed that the lateral displacement experienced by an individual particle as it moves around a cylindrical obstacle is in excellent agreement with such a simple model.[45] In addition, we showed that, even for relatively small separation between the obstacles, a model in which the trajectory is approximated by a series of independent particle-obstacle collisions with asymptotic b_{in} and b_{out} values (dilute-limit approximation for the obstacles), is fairly accurate.[44] This approximation implies that for a given b_c it is also possible to calculate the effective migration angle (α) not only for all forcing directions (θ), but also for any type of lattice or spacing between the obstacles.

For the motion of the drops considered in this work, and as a first approximation motivated by the small Ca numbers, we shall assume that there is no deformation upon the collisions, and use the model described above. In fact, independent of the behaviour of the drops at small separations with the obstacles and their possible deformation, our basic assumption is that collisions can be classified into hydrodynamic ones (no lateral displacement) and touching ones ($b_{out} = b_c$). A second approximation is that consecutive collisions can be treated in the dilute-limit approximation. In Fig. 2 we show that this simple model accurately describes the average migration angle of the drops as a function of the forcing direction for all drops with $\beta \leqslant \delta$. To obtain these theoretical curves we simply calculate b_c from the first critical angle using the relation $b_c = l\sin(\theta_c)$. This equation is obtained by comparing the horizontal displacement (or shift) between obstacles located in successive rows of the array due to the rotation of the device, with the lateral displacement experienced by a drop as a result of a touching collision (see Fig. 6). As shown in Fig. 6, for $\theta < \theta_c$ the drop is clearly locked in the [0,1] direction, falling down a single column of the array. Only when for $\theta > \theta_c$ does the drop finally move across a column in the device, as shown in Fig. 6b. In terms of the model, all locking directions observed at higher forcing angles, as well as the transition angles between these locking directions, can be predicted from this first transition angle.

The motion of drops that are larger than the separation between cylindrical pegs cannot be described as a series of individual collisions with a single obstacle at a time, and the proposed model is not valid in this case. The dependence of the migration angle on the forcing angle exhibited by such large drops, however, is similar to that observed in the case of smaller

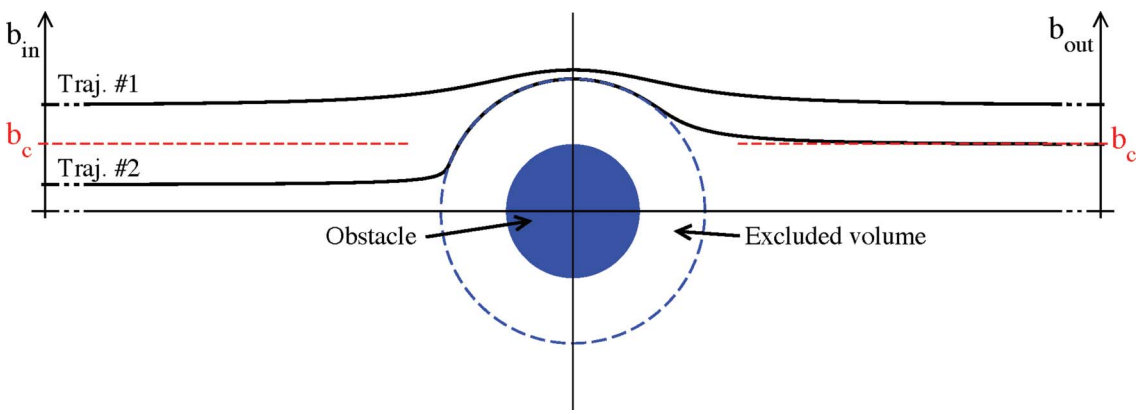

Fig. 5 Schematic view of the trajectory followed by a suspended particle during two different particle–obstacle collisions for $\beta = 1$. A symmetric hydrodynamic collision (trajectory #1) with $b_{in} > b_c$ and $b_{out} = b_{in}$, and a touching collision (trajectory #2) with $b_{in} < b_c$ and $b_{out} = b_c$.

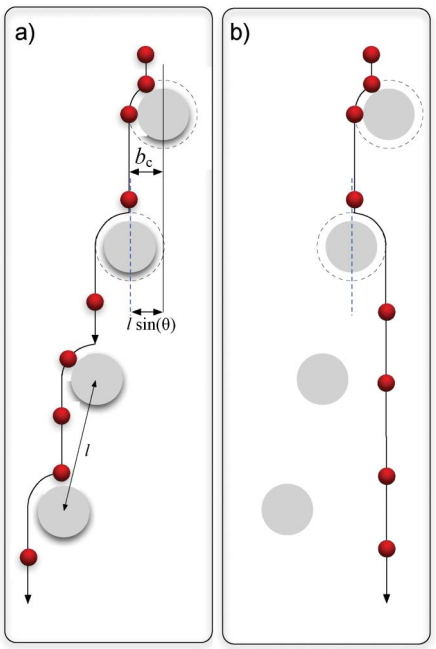

Fig. 6 Schematic view of the single column experiments, showing the settling of a train of drops in a case (a) when the rotation of the board is below and the drops are continuously displaced and (b) an angle higher than the critical value for which $b_c < l\sin(\theta_c)$ and the train of drops goes through the column.

drops, showing directional locking and sharp transitions of the migration angle between locking directions. The 9.3 mm drops (which are larger than the gap between obstacles, $\beta = 1.19$) still show an intermediate locking direction (between [0,1] and [1,1]), that is for $\theta \approx 30^\circ$ the migration angle is $\alpha = 26.56^\circ$, corresponding to the [1,2] direction. Also, in agreement with the results for smaller drops, the larger drops display increasing values of the first critical angle with drop size. This shows that, as expected, it is increasingly difficult for a drop to move across a column of obstacles in the device for $\beta > \delta$.

2.4 Single line experiments

An interesting test for the validity of the proposed model based on the dilute-limit approximation is that it predicts that a single line of obstacles would be sufficient to perform a binary fractionation of a mixture of drops. Specifically, a line of obstacles separated by the same distance l as in the array and oriented at some angle θ with respect to the forcing direction would deflect all those drops for which $\theta_c > \theta$, but let smaller drops with $\theta_c < \theta$ go through, as represented in Fig. 6 (Note that Fig. 6 shows the behaviour of a given drop size for two different forcing angles but it is analogous to the case of a given forcing angle and two drop sizes.) In certain situations, it could be advantageous to use a single line of obstacles instead of the entire array. For example, it would be straightforward to create a series of individual lines at different orientations to perform more complex fractionations. More importantly, if the dilute-limit approximation is valid we could then predict the migration angle of a drop for any geometrical arrangement of the obstacles (periodic or not), solely based on the measured value of the first critical angle. In that case, it would be possible to optimize the pattern in which the obstacles are positioned for each sample to be fractionated using simple geometrical considerations. Therefore, to test our model, we performed single line experiments in which only one line of obstacles is used from the original square lattice. In these experiments we rotate the device starting from $\theta = 0^\circ$ and measure the first angle at which the drops go through the line of obstacles. According to the proposed model this angle should be equal to the critical angle θ_c measured in the array. The critical angles measured using a single line of obstacles are shown in Fig. 3. They clearly agree with the critical angles measured using the square array of obstacles. Surprisingly, there is good agreement even in the case of large drops, where one could have expected the two cases (single line *vs.* array) to have different critical angle, due to the interaction of the drop with multiple obstacles simultaneously. In addition, the fact that different drop sizes have different critical angles implies that a single line of obstacles can be employed for binary separation.

The experiments discussed above demonstrates that the critical angle for drops moving past a single column of obstacles is the same as the critical angle for the full array. However, there could be a dependence of the critical angle on the separation between the obstacles. In particular, it would be natural to expect such a dependence of the critical angle on the separation between obstacles in the case of relatively large drops, when their size is similar to the gap between pegs. Therefore, to further test the limitations of the dilute approximation we performed a separate set of single line experiments in which we doubled the separation between obstacles to $2l$. As shown in Fig. 3 the critical angles are different in this case, compared to those obtained in the original array. This is expected, given that the critical angle is not a local quantity but depends on the geometry of the array (*e.g.* on the distance and relative position of the obstacles.) On the other hand, the critical impact parameter should only depend on the drop-obstacle pair and not on the location of other obstacles. In fact, when we plot the corresponding critical impact parameter,

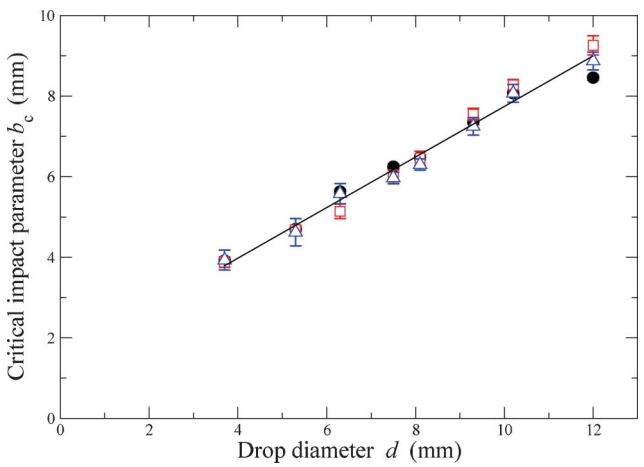

Fig. 7 Critical impact parameter as a function of drop diameter. The solid symbols correspond to the measurements in the array and the open squares (triangles) correspond to single row experiments with separation l ($2l$) between the pegs. The solid line is a linear fit $b_c = 1.5 + 1.25\ (d/2)$, with a correlation coefficient $R = 0.991$.

b_c in Fig. 7, we observe excellent agreement for all three sets of experiments. Again, the observed agreement extends well beyond the range of drop sizes for which a dilute approximation is valid. We also show that a linear dependence is a good approximation for the critical impact parameter as a function of the drop size.

3. Conclusions

We have shown that force-driven deterministic lateral displacement (*f*-DLD) is a promising technique for the separation of drops. We performed macroscopic experiments using a scaled-up microfluidic device consisting of a square array of cylindrical obstacles. We investigated the average migration angle of a wide range of drops sizes, including large ones that deform considerably as they move through the array. The results presented here were performed in the deterministic limit, and at small Reynolds and capillary numbers, which makes them a suitable model for microfluidic devices. In all cases we observe the presence of directional locking, in which the drops migrate at selected lattice directions, analogous to the motion observed with solid particles. We showed that a simple model based on individual obstacle-drop collisions, in which the first critical angle is the only fitting parameter, accurately described the observed locking behaviour for all forcing angles. From these experiments we obtained important design criteria for the fabrication of *f*-DLD devices for drop separation. Firstly, the large window in forcing angles observed (approximately 20°) makes the first transition the best suited for separation purposes. Secondly, the considerable reduction in the average velocity that the drops experience when the forcing direction is close to any of the critical angles suggests that the average velocity itself can be used to enhance separation resolution and capacity. Thirdly, we demonstrated that it is possible to use a single line of cylindrical obstacles to perform binary separations. Finally, the agreement between the critical angles measured with a single line of obstacles with those determined using the full array allows for the selection of the optimal lattice structure and spacing solely based on geometrical considerations. Increasing the spacing between obstacles, for instance, would provide a straightforward strategy to reduce the occurrence of clogging in the microdevices.

Acknowledgements

This material is based upon work partially supported by the National Science Foundation under Grant Nos. CBET-0933605, CMMI-0748094, and CBET-0954840.

References

1 G. M. Whitesides, *Nature*, 2006, **442**, 368–373.
2 M. U. Kopp, H. J. Crabtree and A. Manz, *Curr. Opin. Chem. Biol.*, 1997, **1**, 410–419.
3 P. A. Auroux, D. Iossifidis, D. R. Reyes and A. Manz, *Anal. Chem.*, 2002, **74**, 2637–2652.
4 D. R. Reyes, D. Iossifidis, P. A. Auroux and A. Manz, *Anal. Chem.*, 2002, **74**, 2623–2636.
5 M. A. Schwarz and P. C. Hauser, *Lab Chip*, 2001, **1**, 1–6.
6 S. Haeberle and R. Zengerle, *Lab Chip*, 2007, **7**, 1094–1110.
7 T. Kulrattanarak, R. G. M. van der Sman, C. G. P. H. Schroen and R. M. Boom, *Adv. Colloid Interface Sci.*, 2008, **142**, 53–66.
8 J. A. Bernate and G. Drazer, *J. Colloid Interface Sci.*, 2011, **356**, 341–351.
9 N. Pamme, *Lab Chip*, 2007, **7**, 1644–1659.
10 M. Kersaudy-Kerhoas, R. Dhariwal and M. P. Y. Desmulliez, *IET Nanobiotechnol.*, 2008, **2**, 1–13.
11 A. Lenshof and T. Laurell, *Chem. Soc. Rev.*, 2010, **39**, 1203–1217.
12 L. R. Huang, E. C. Cox, R. H. Austin and J. C. Sturm, *Science*, 2004, **304**, 987–990.
13 S. Y. Zheng, R. Yung, Y. C. Tai andH. Kasdan, Deterministic lateral displacement MEMS device for continuous blood cell separation, *Micro Electro Mechanical Systems, 2005. MEMS 2005. 18th IEEE International Conference on*, 30 Jan.-3 Feb. 2005, pp. 851–854, DOI:10.1109/MEMSYS.2005.1454063, URL:http://ieeexplore.ieee.org/stamp/stamp.jsp?tp=&arnumber=1454063&isnumber=31227.
14 N. Li, D. T. Kamei and C. M. Ho, On-Chip Continuous Blood Cell Subtype Separation by Deterministic Lateral Displacement,*Nano/Micro Engineered and Molecular Systems, 2007. NEMS '07. 2nd IEEE International Conference on*, 16-19 Jan. 2007, pp. 932–936, DOI:10.1109/NEMS.2007.352171, URL:http://ieeexplore.ieee.org/stamp/stamp.jsp?tp=&arnumber=4160474&isnumber=4144525.
15 K. J. Morton, K. Loutherback, D. W. Inglis, O. K. Tsui, J. C. Sturm, S. Y. Chou and R. H. Austin, *Lab Chip*, 2008, **8**, 1448–1453.
16 D. W. Inglis, K. J. Morton, J. A. Davis, T. J. Zieziulewicz, D. A. Lawrence, R. H. Austin and J. C. Sturm, *Lab Chip*, 2008, **8**, 925–931.
17 J. V. Green, M. Radisic and S. K. Murthy, *Anal. Chem.*, 2009, **81**, 9178–9182.
18 D. W. Inglis, N. Herman and G. Vesey, *Biomicrofluidics*, 2010, **4**, 024109.
19 H. N. Joensson, M. Uhlen and H. A. Svahn, *Lab Chip*, 2011, **11**, 1305–1310.
20 S. H. Holm, J. P. Beech, M. P. Barrett and J. O. Tegenfeldt, *Lab Chip*, 2011, **11**, 1326–1332.
21 D. W. Inglis, M. Lord and R. E. Nordon, *J. Micromech. Microeng.*, 2011, **21**, 054024.
22 Z. G. Li and G. Drazer, *Phys. Rev. Lett.*, 2007, **98**, 050602.
23 D. R. Gossett, W. M. Weaver, A. J. Mach, S. C. Hur, H. T. K. Tse, W. Lee, H. Amini and D. Di Carlo, *Anal. Bioanal. Chem.*, 2010, **397**, 3249–3267.
24 J. P. Beech and J. O. Tegenfeldt, *Lab Chip*, 2008, **8**, 657–659.
25 K. J. Morton, K. Loutherback, D. W. Inglis, O. K. Tsui, J. C. Sturm, S. Y. Chou and R. H. Austin, *Proc. Natl. Acad. Sci.*, 2008, **105**, 7434–7438.
26 B. R. Long, M. Heller, J. P. Beech, H. Linke, H. Bruus and J. O. Tegenfeldt, *Phys. Rev. E.*, 2008, **78.**
27 T. Kulrattanarak, R. G. M. van der Sman, C. Schroen and R. M. Boom, *Microfluid. Nanofluid.*, 2011, **10**, 843–853.
28 T. Kulrattanarak, R. G. M. van der Sman, Y. S. Lubbersen, C. Schroen, H. T. M. Pham, P. M. Sarro and R. M. Boom, *J. Colloid Interface Sci.*, 2011, **354**, 7–14.
29 M. Balvin, E. Sohn, T. Iracki, G. Drazer and J. Frechette, *Phys. Rev. Lett.*, 2009, **103.**
30 J. Herrmann, M. Karweit and G. Drazer, *Phys. Rev. E.*, 2009, **79.**
31 Y. S. Lubbersen, M. A. I. Schutyser and R. M. Boom, *Chem. Eng. Sci.*, 2012, **73**, 314–320.
32 R. Seemann, M. Brinkmann, T. Pfohl and S. Herminghaus, *Rep. Prog. Phys.*, 2012, **75**, 16601–16601.
33 S.-Y. Teh, R. Lin, L.-H. Hung and A. P. Lee, *Lab Chip*, 2008, **8**, 198–220.
34 M. Chabert and J.-L. Viovy, *Proc. Natl. Acad. Sci.*, 2008, **105**, 3191–3196.
35 D. Huh, J. H. Bahng, Y. B. Ling, H. H. Wei, O. D. Kripfgans, J. B. Fowlkes, J. B. Grotberg and S. Takayama, *Anal. Chem.*, 2007, **79**, 1369–1376.
36 D. R. Link, E. Grasland-Mongrain, A. Duri, F. Sarrazin, Z. D. Cheng, G. Cristobal, M. Marquez and D. A. Weitz, *Angew. Chem., Int. Ed.*, 2006, **45**, 2556–2560.
37 Y. C. Tan and A. P. Lee, *Lab Chip*, 2005, **5**, 1178–1183.
38 R. Quek, D. V. Le and K. H. Chiam, *Phys. Rev. E.*, 2011, **83**, 056301.
39 J. P. Beech, S. H. Holm, K. Adolfsson and J. O. Tegenfeldt, *Lab Chip*, 2012, **12**, 1048–1051.
40 T. M. Squires and S. R. Quake, *Rev. Mod. Phys.*, 2005, **77**, 977–1026.
41 P. Garstecki, M. J. Fuerstman, H. A. Stone and G. M. Whitesides, *Lab Chip*, 2006, **6**, 437–446.
42 P. Bak, *Rep. Prog. Phys.*, 1982, **45**, 587–629.
43 J. Koplik and G. Drazer, *Phys. Fluids*, 2010, **22**, 052005.
44 J. Frechette and G. Drazer, *J. Fluid Mech.*, 2009, **627**, 379–401.
45 M. Luo, F. Sweeney, S. R. Risbud, G. Drazer and J. Frechette, *Appl. Phys. Lett.*, 2011, **99**, 064102.

